Locating and quantifying necking in piles through numerical simulation of PIT

T. Salem, A. Eraky, A. Elmesallamy
Faculty of Engineering, Zagazig University, Zagazig, Egypt.
nageeb2@yahoo.com, 0020-100-7040-659
atef_eraky@yahoo.com , 0020-100-5283-557
almosllamy@gmail.com, 0020-102-2011-122

ABSTRACT. Defects of concrete piles can occur at any point during the construction of piles. Most common types of pile integrity issues are; presence of voids, inconsistency in concrete mix, entrapped groundwater or slurry, and geometric dislocation. These defects can be categorized based on the place in the construction sequence at which the defect occurs. This research introduces several numerical models of defected piles with various scenarios in order to identify, locate, and quantify the necking occurring in these piles. The finite element software (ADINA) is used to simulate the studied models. The soil domain is modeled as an axisymmetric space around the concrete pile. Five diameters of piles (40, 60, 80, 100 and 120 cm) are studied. Necking is modeled at three different locations along the pile namely; upper, middle, and bottom third. Four ratios between the necking diameter and pile diameter are also studied. The dynamic force used in this research is that simulating the pile integrity test (PIT) case, with 2.5 N impact load applied at the pile head, half wave of sinusoidal pattern, and 0.5 kilo hertz frequency. The time domain of the dynamic force analysis is equal to 0.0175 sec, and applied in 450 steps.

KEYWORDS. Pile integrity test; Damage detection; Necking in piles.

INTRODUCTION

There are many shapes of defects in concrete piles such as; cracking, honey-combing, bulges, and necking. Necking is a reduction in cross sectional area of the pile, while bulges are increases in the pile cross sectional area. The integral (healthy) pile is that one having constant diameter along its whole length with no cracks, necking, bulges, or honey-combing. Non-destructive tests with dynamic loads are used to predict the location of pile defects. One of the most familiar tests used for this target is the pile integrity test (PIT), which is fast, common, and low-cost test. The mechanism of (PIT) is that the wave transfer from pile head to pile toe then return to the top. Although, the (PIT) is a fast and reliable test, there are some shortcomings of this test.

Štrukelj et al., (2009) introduced a monitoring methodology where sensors are installed inside the pile body to measure the pile strain under dynamic load. The results of the experiment are compared with a numerical model conducted by PLAXIS software. Trauner (2012) studied the behavior of reinforced concrete pile inside a soil domain under dynamic load. Sensors are installed on the steel reinforcement bars to measure the strain of the pile. Furthermore, verification is conducted with a real PIT carried out on the field.

Ding et al., (2011) studied the PIT wave propagation in a tube section pile numerically. Models are carried out with different wall thickness and different elastic moduli. Niederleithinger (2006) and (2008) described the CEFIT software to simulate the PIT and the acoustic wave through the pile and the soil. Zhang et al., (2010) used ANNs software to simulate the PIT with neural network technique. Warrington and Wynn (2000) studied the difference between the software MAPLE, ANSYS and WEAP, in simulating wave equation through concrete piles.

Li, (2019) studied large-diameter pipe pile embedded in inhomogeneous soil to investigate the torsional dynamic response, and presented verification of the frequency-domain analytical solution. The author concluded that with increasing the inner radius and length of the pile or the decrease of the outer radius and shear modulus of the pile, the oscillation amplitudes of the complex impedance and velocity admittance decrease, denoting an increase in the resistance of the pile
to torsional dynamic loadings.

Wu et al., (2019) study the longitudinal vibration of a pile with changeable sectional acoustic impedance under arbitrary external stimulation. The Laplace transform is used to find the analytical solution of the transfer function, and then the residue technique of inverse Laplace transformation is used to solve the corresponding impulse response function. The analytical solution of response at pile top may be found by convolution computation using the impulse response function, which overcomes the limit of earlier analytical solutions due to defined time-harmonic load.

Li and Gao, (2019) introduced better approach for describing the vertical vibration of a pipe pile while taking into account the layered characteristics and building disturbance impact of both the outer and inner soils for various pile specifications and soil radial inhomogeneity conditions, the impacts of the inner soil on the dynamic response of the pipe pile were explored. The theoretical model's accuracy was confirmed by comparing the outcomes of field measurements.

This paper studies different models of concrete piles having different necking locations and sizes using ADINA (2021) software. Several scenarios of piles with necking defect are studied. The pile necking diameter is modeled with four different values at three different locations along the pile length. The velocity response for an arbitrary point on the pile surface is plotted with the time. The main objective of this study is to introduce a new methodology to locate and quantify necking in piles with a new standard graph as a reference.

MODELING

Studied concrete piles are considered to have circular cross-sectional area and totally embedded in the soil. The pile radii varied from 40 to 120 cm, with all having the same length of 12 meters. An axisymmetric model is used in modeling the pile and the surrounding soils, with soil domain radius equal to 24 m plus the pile diameter, and a height of 24 m. The same meshing pattern is used in all the models having the same incremental values, sequence, and order, thus, avoiding the effect of meshing on the results. Tab. (1) presents the properties of the soil and the pile materials used in the numerical analysis.

Materials	Numerical model	Young's Modulus (MN/m²)	Density (kg/m³)	Poisson's Ratio	Friction Angle (o)
Concrete	Elastic isotropic	2.1×10^3	2500	0.2	N/A
Soil	Mohr-Coulomb	1.0×10^2	1900	0.3	40

Table 1: Properties of the Studied Soil and Concrete Materials.

A very small value of Rayleigh damping stiffness factor β for the pile is assumed $= 70 \times 10^{-7}$, while Rayleigh damping mass factor α for the pile is assumed to be zero. In addition, Rayleigh damping stiffness factor β and mass factor α for the soil is considered $= 0$. These very small values are mainly chosen due to the very short duration of monitoring the incident wave, so that it's considered that the damping effect will not affect the behavior before a relatively long duration.

The dynamic load used in this research is an impact load. It modeled in ADINA software as concentrated load equal to 2.5 N applied at the pile head, with time function as presented in Fig. (1). The considered solution steps are 50 steps during the pulse duration which equals 0.001 sec, then 400 steps from 0.001 sec to 0.017 sec. For solving the finite element equations in a linear dynamic analysis, ADINA employed the step-by-step direct integration through implicit time integration using the Newmark's method.
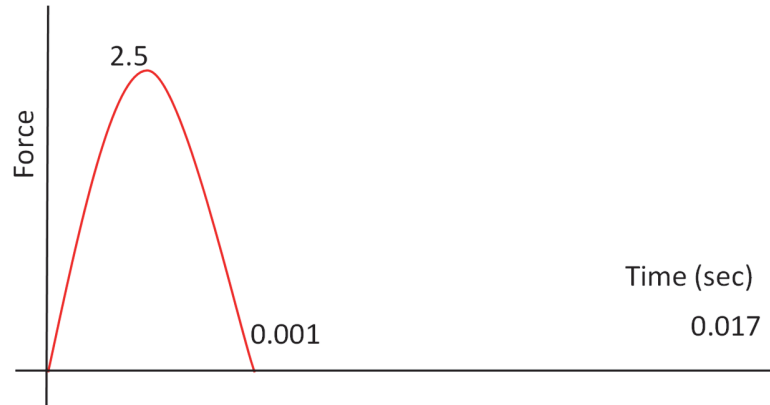
Figure 1: Force Time Function of Dynamic Load.

The model increases laterally every 60 cm to respect the condition (mesh side should have a maximum length = $C \times t_c / 2.5$). The wave velocity $(C) = \sqrt{E/\varrho}$, where E is the concrete Young's modulus and ϱ is the concrete density. Therefore, the wave velocity is taken equal to 3000 m/s. The time of impact load is 0.001 sec of a half sinusoidal wave and frequency 0.5 kHz. Lateral and cross-sectional meshes have the same dimensions at the necking zone. The element size within the mesh surrounding the pile is equal to 5 cm in both directions. 3D-model of the pile and the surrounding soil is shown in Fig. (2).
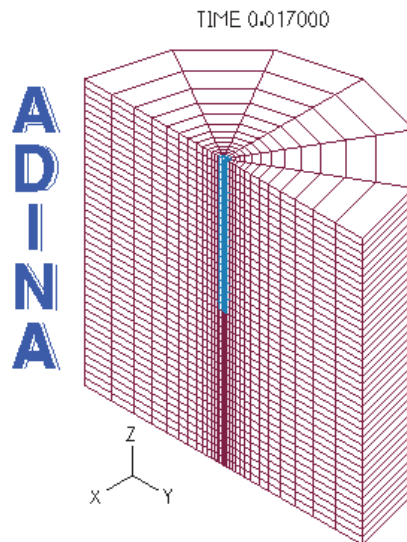
Figure 2: Finite Element Axisymmetric Model for the Intact Pile Case.

Regarding the boundary conditions, the bottom boundary is fixed with no movements in X, Y, and Z directions. However, the side boundaries are rollers in the vertical directions to allow for soil settlement, as shown in Fig. (3). Larger mesh sizes are used in the analysis to assess the effect of mesh size convergence. The chosen mesh size along with the FEM discretization showed no difference in the results between the used mesh and the smaller ones indicating the accuracy of the used mesh. This may be attributed to the relatively short time of solution which is 0.017 sec also the relatively low applied point load value which is 2.5 N to the model mass.
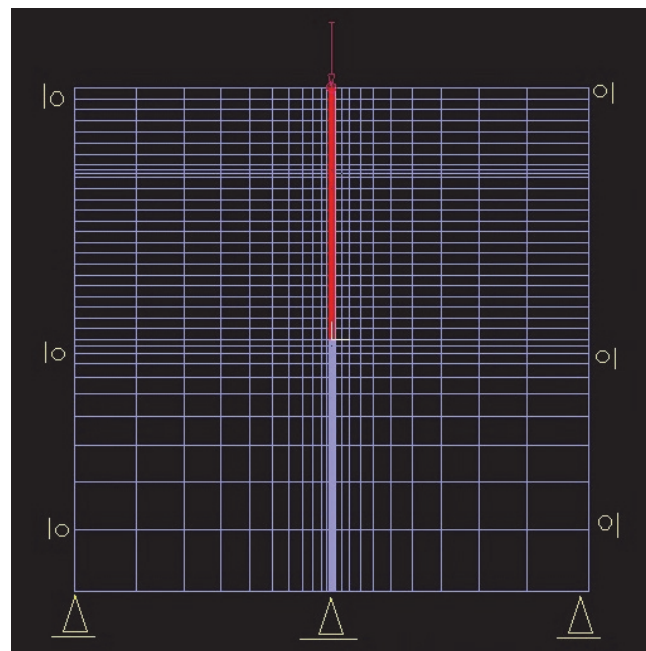
Figure 3: Boundary conditions of the Finite Element.

STUDIED CASES

A parametric study is performed in which the following parameters are studied in details:
Pile diameter varying from 40, 60, 80, 100 and 120 cm. Notch or necking in three different locations, upper, middle third, and lower third. Four notch or necking sizes, as reduced from the pile diameter, having sizes of 12.50%, 25.0%, 37.5%, and 50.0% are deducted as notch from the pile diameter.

RESULTS

Relationship between time and velocity at a specific point are studied for all cases. The location of the studied point is at (1/3 * pile radius) from the pile center. Different parameters are studied, including pile diameter, necking diameter, and the ratio between them. Obtained curves are compared with the PIT manual schematic diagram.
Fig. (4) shows the velocity time history at the studied point located on the surface of intact pile with diameter = 100 cm. It is found that there are two marked parabolas (a and z). Parabola (a) is the pulse induction and named as the initial parabola in the paper. Initial parabola is induced directly due to the impulse effect not as the same parabolas along the response history which induced after the pulse release. Initial parabola was found as smooth peak in smaller diameters 40 cm and 60 cm and gradually noised from 60 cm then 80 cm then 100 cm then 120 cm. This declares the direct relation between the pulse frequency effect on the PIT test and gives an obvious observation that for every pile diameter there is an optimum frequency. parabola (z) is the terminal parabola or the end parabola, and it means that the wave has reached the pile end and reflect. The symbol t_{lp} in Fig. (4) expresses the time indicating the distance between the pile head and its end bearing point along the whole pile length. The end parabola will show a conclusion as its trend is affected by necking and also its shape changes with noisy waves in the initial parabolas. In addition, it should be noted that the responses don't drop down to less than zero from time $2*10^{-3}$ sec to time $8*10^{-3}$ sec.
Fig. (5) presents a comparison of velocity time history between intact pile with D = 100 cm and four different necking values. All four necked piles have a necking at the upper third zone of the pile length. The necked pile diameters are 87.5, 75.0, 62.5 and 50.0 cm, with diameter reduction of 12.5, 25.0, 37.5, and 50.0 cm respectively. The symbol t_{lu} in Fig. (5) expresses the time indicating the distances between the pile head and the necking location. The symbol t_{lp} in Fig. (5) expresses the time indicating the distance between the pile head and its end bearing point along the whole pile length. It is

noticed that the part [Q] of the graph increases downward when the pile diameter decreases, or when the necking increases.
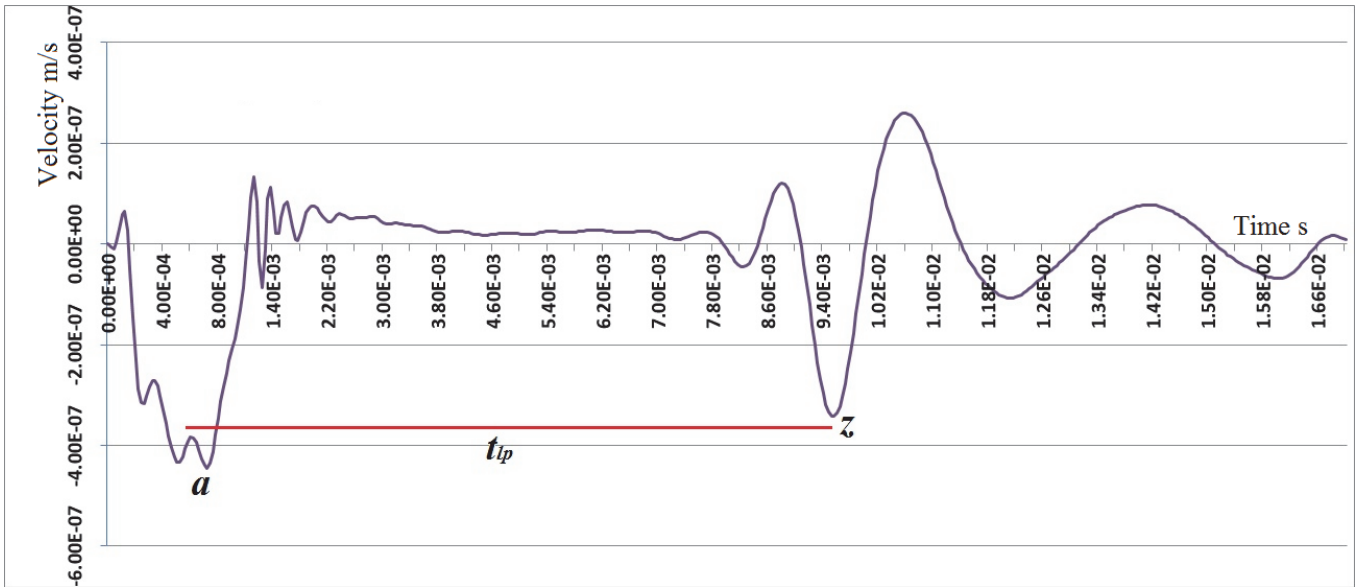

Figure 4: Velocity Response for an Intact Pile of 100 cm Diameter.
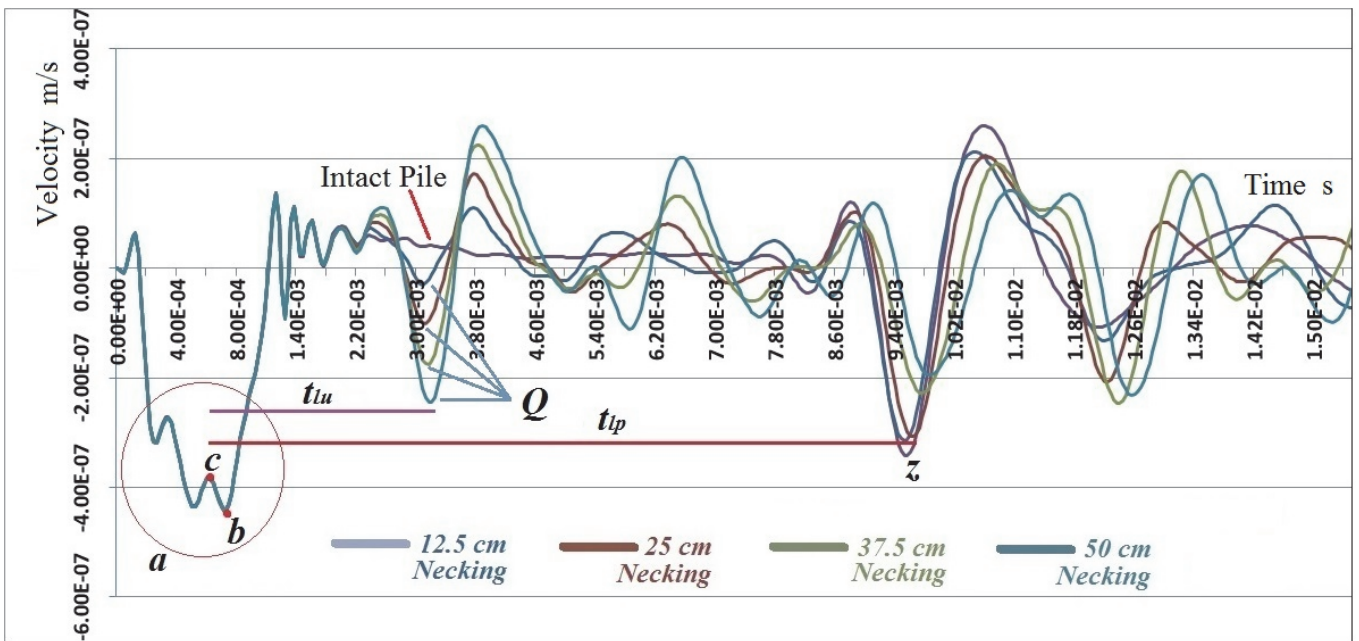

Figure 5: Velocity Response for an Intact Pile 100 cm Diameter verses Four Defected Piles at Upper Third of the Pile Length.

In which:

Q   : is the negative peak velocity just after the initial zone, (m/sec.);
a   : is the zone of noise that took place in the initial parabola;
b   : is the lowest peak in the initial noise zone;
c   : is a noise point just preceding the lowest peak in the initial noise zone.

Fig. (6) presents a comparison of velocity time history between intact pile (D = 100 cm) and four necked piles. All four necked piles have a neck at the middle of the pile length. The necked pile diameters are 87.5, 75.0, 62.5 and 50.0 cm. The

symbol t_{lm} in Fig. (6) expresses the time indicating the distances between the pile head and the necking location. It is noticed that part [P] of the graph increases downward when the pile diameter decreases, or when the necking increases.
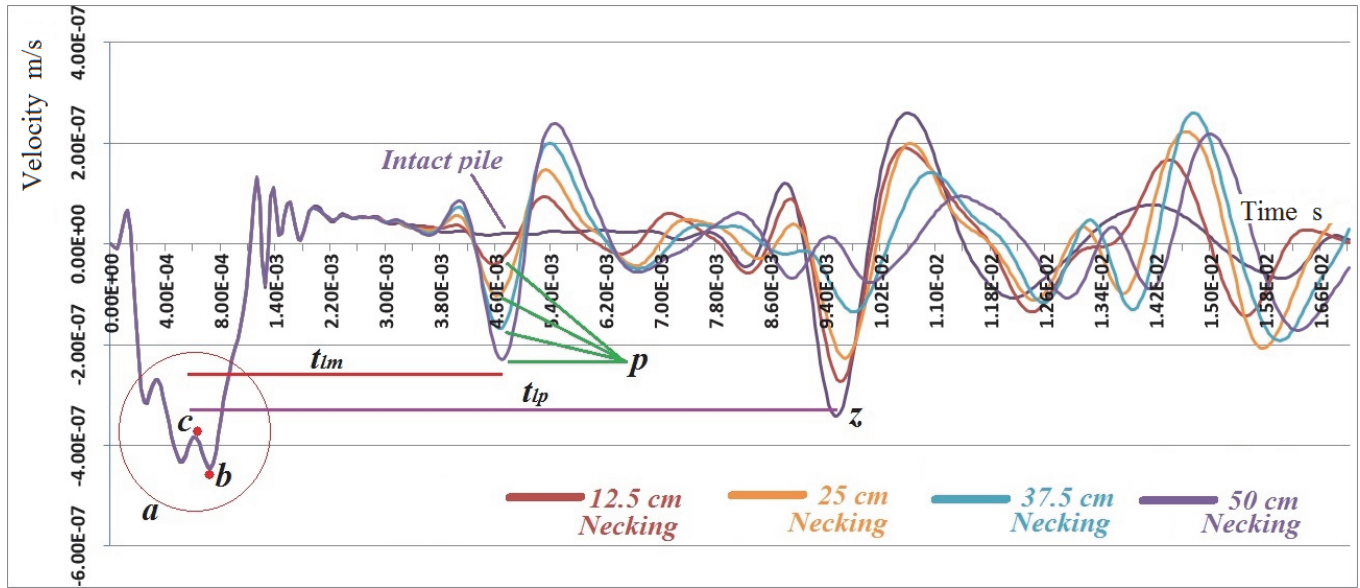

Figure 6: Velocity Response for an Intact Pile 100 cm Diameter Verses Four Defected Piles at the Middle of the Pile Length.

Fig. (7) shows a comparison of velocity time history between the case of intact pile (D = 100 cm) and four necked piles with a neck at the lower third part of the pile length. The same necking ratios are used in this case also. The symbol t_{lb} in Fig. (7) expresses the time that the wave travels over the first two thirds of the pile. It is noticed that the part [O] of the graph increases downward when the pile diameter decreases, or when the necking increases.
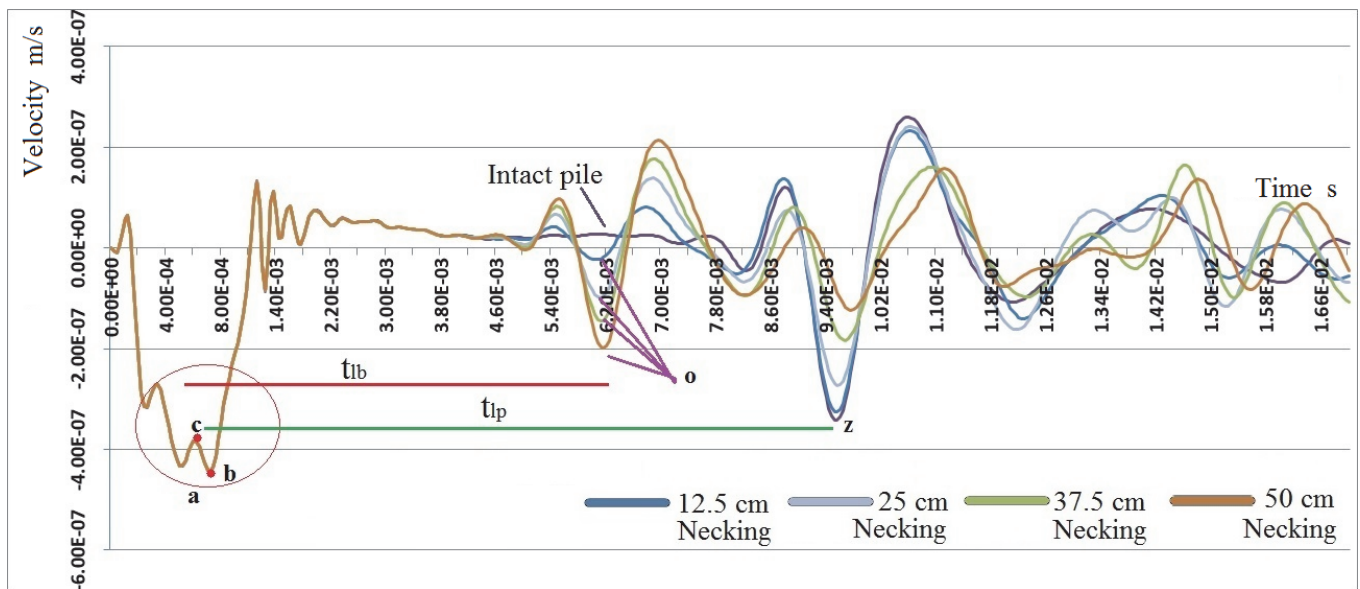

Figure 7: Velocity Response for an Intact Pile 100 cm Diameter Verses Four Defected Piles at the Lower Third of the Pile Length.

Fig. (8) summarizes Figs. (4), (5), and (6). It is noticed that there is a time shift on the velocity time history curves when the location of the necking moves from the pile top to the pile middle or the pile bottom. The distance between the domain values is t_{lu}, t_{lm}, t_{lb} are proportional to the physical distances between the necking in the pile to the pile length expressed in the pile length domain value t_{lp}.
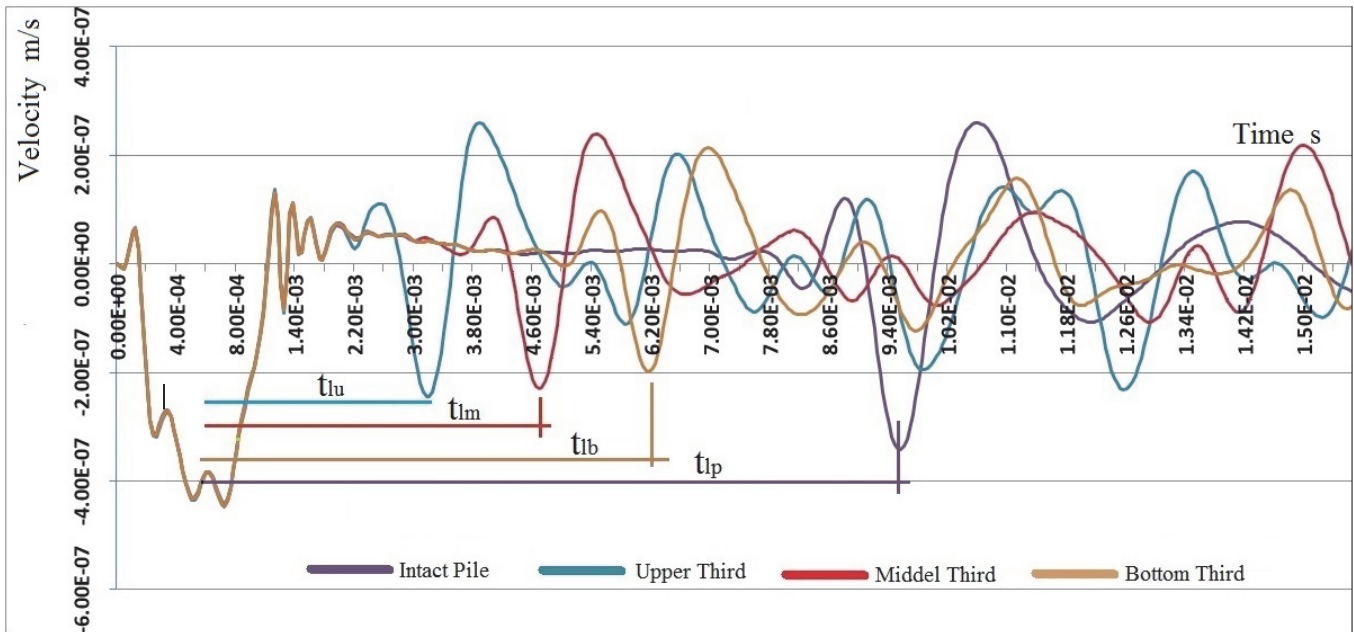
Figure 8: Velocity Response for an Intact Pile 100 cm Diameter Verses Three Defected Piles of 50 cm Necking at Upper, Middle and Lower Third of the Pile Length.

The behavior of the studied piles has a pattern which can be presented in Fig. (10). It may be compared with the known PIT manual shape which passes through several operations of filtration and other mathematical computations to specify the defect location, as shown in Fig. (9).
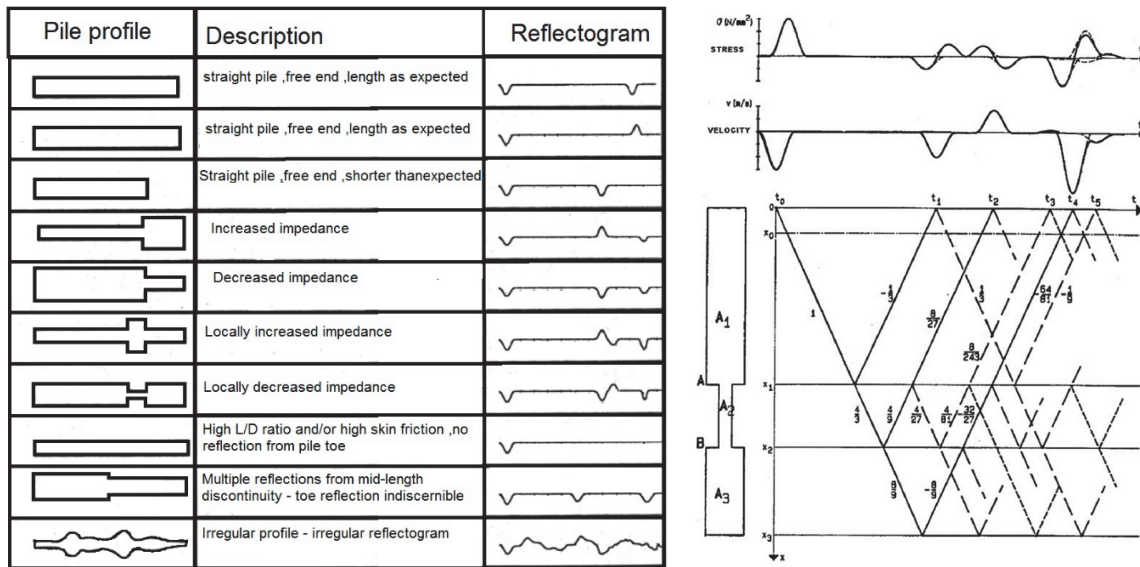

Figure 9: The PIT Schematic Diagram and Table.

The research schematic diagram has a new conclusion that it may introduce approximately the volume of the defect. In addition, it doesn't need any computations for filtration, but just the direct introduced response and comparing the result with the new schematic diagram, as presented in Fig. (10). On other hand, it can be said that the ratio between the notch diameter to the pile diameter is approximately equal to the ratio shown in the following equation:

$$RD = \frac{y_1}{2*y_2 - y_3}$$

(1)

where:

y_1 : is the peak velocity of parabola [Q],

y_2 : is the velocity value at point [b],

y_3 : is the velocity value at point [c].

a, Q, b, and c are presented in Figs. (5) and (10).

y_2 or (b) is the minimum value in the pulse parabola [a] and y_3 or (c) is the maximum y value in the pulse parabola [a]. It can be predicted whether the pile is intact or not using this formula. In addition, the location and the diameter of the necking can also be predicted.
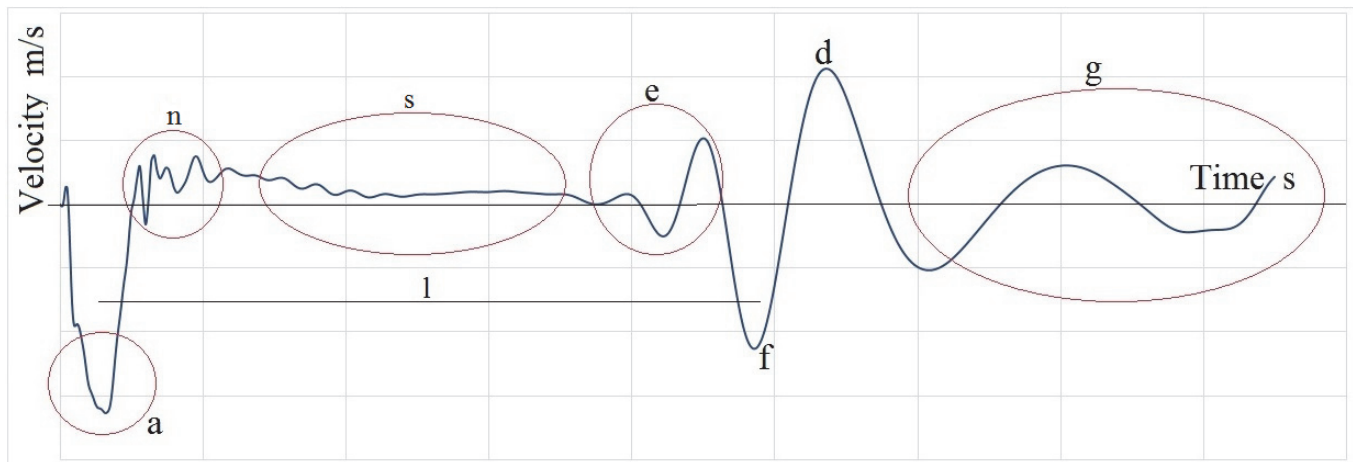

Figure 10: The Research Schematic Diagram.

a: Impact peak.

n: Noisy portion directly after impact peak

s: Studied portion.

d: Maximum positive amplitude along the response whatever its duration.

L: Scoped response length

f: Minimum negative amplitude along the response whatever its duration.

e: Noisy portion directly beyond the minimum velocity response value.

g: Noisy portion directly after maximum velocity response value.

EFFECT OF PILE DIAMETER

The effect of pile dimeter is shown in the following figures, knowing that the figures having similar trends of that of 100 cm pile diameter. Fig. (11) presents a comparison of velocity time history between intact pile with D = 40 cm and four piles having different necking. All four necked piles have a neck at the upper third of the pile length. The necking (or reduction) in the pile diameter is 5, 10, 15 and 20 cm respectively. It is noticed that the part [Q] of the graph increases downward when the pile diameter decreases, or when the necking increases.

It is noticed that for pile diameters of 40 and 60 cm, shown in Figs. (11) and (12), a separate single parabola with no inflection point appeared below the pile tip for the intact pile only in the negative zone. On the other hand, all piles with different necking zones are having one or more inflection points with much more distorted parabolas for larger necking zones. However, for pile diameters of 80, 100, and 120 cm, the peak of the parabola appeared in the positive zone just below the pile tip also. This may be attributed to that the frequency in the initial parabola induced a significant noise in larger diameters, as shown in Figs. (5), (13), and (14).

The same trend is noticed for different pile diameters, and shown in successive figures, Fig. (12) for 60 cm diameter pile, Fig. (13) for 80 cm diameter pile, and Fig. (14) for 120 cm diameter pile.
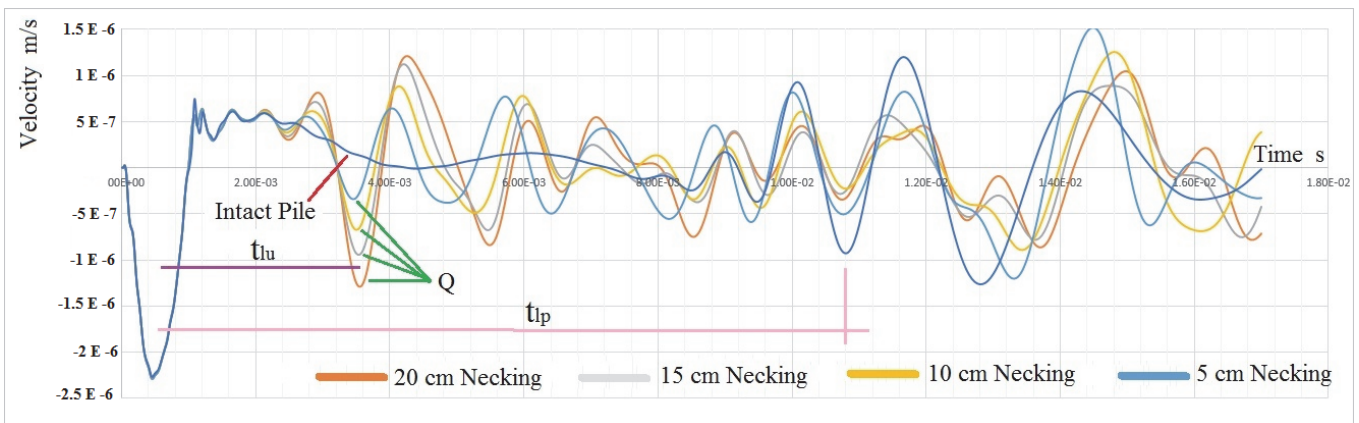
Figure 11: Velocity Response for an Intact Pile 40 cm Diameter Verses Four Defected Piles at the Higher Third of the Pile Length.
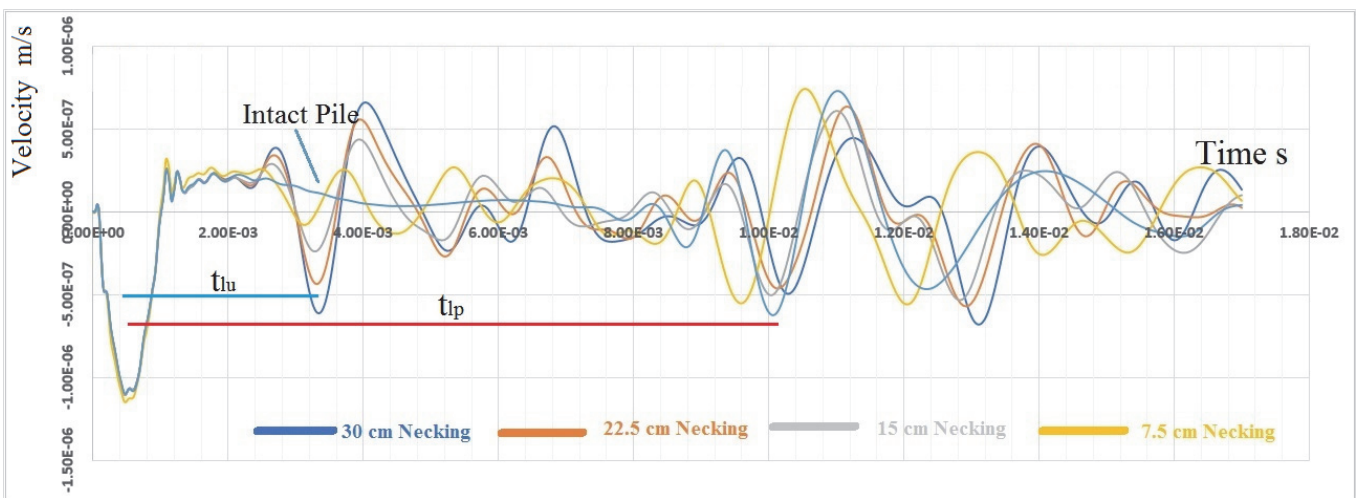

Figure 12: Velocity Response for an Intact Pile 60 cm Diameter Verses Four Defected Piles at the Upper Third of the Pile Length.
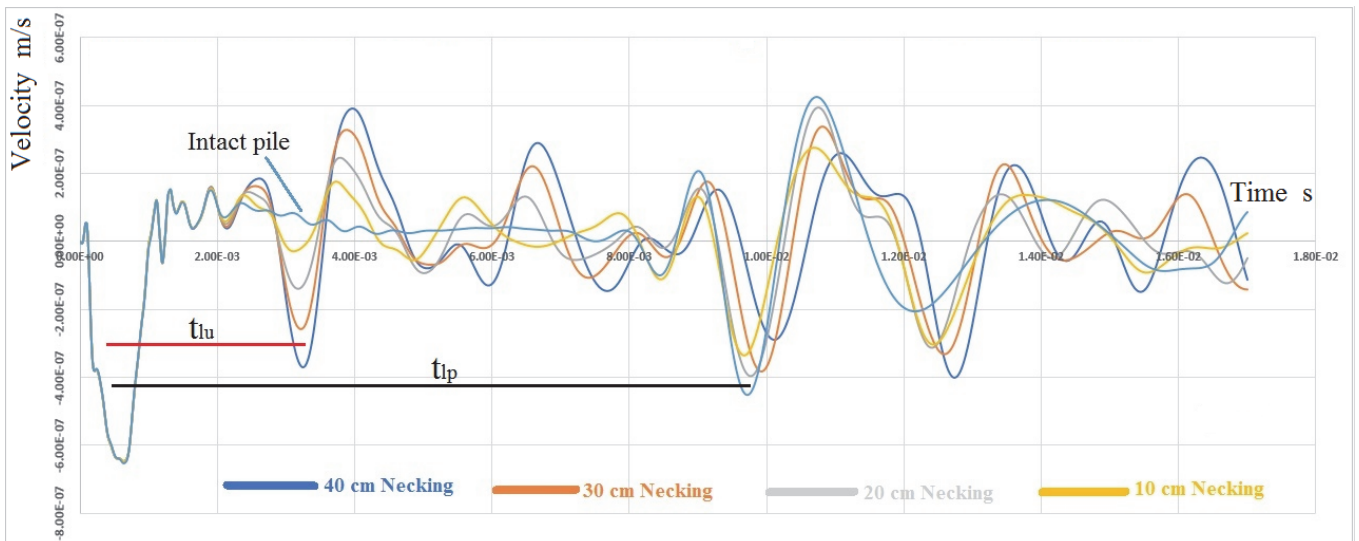

Figure 13: Velocity Response for an Intact Pile 80 cm Diameter Verses Four Defected Piles at the Upper Third of the Pile Length.
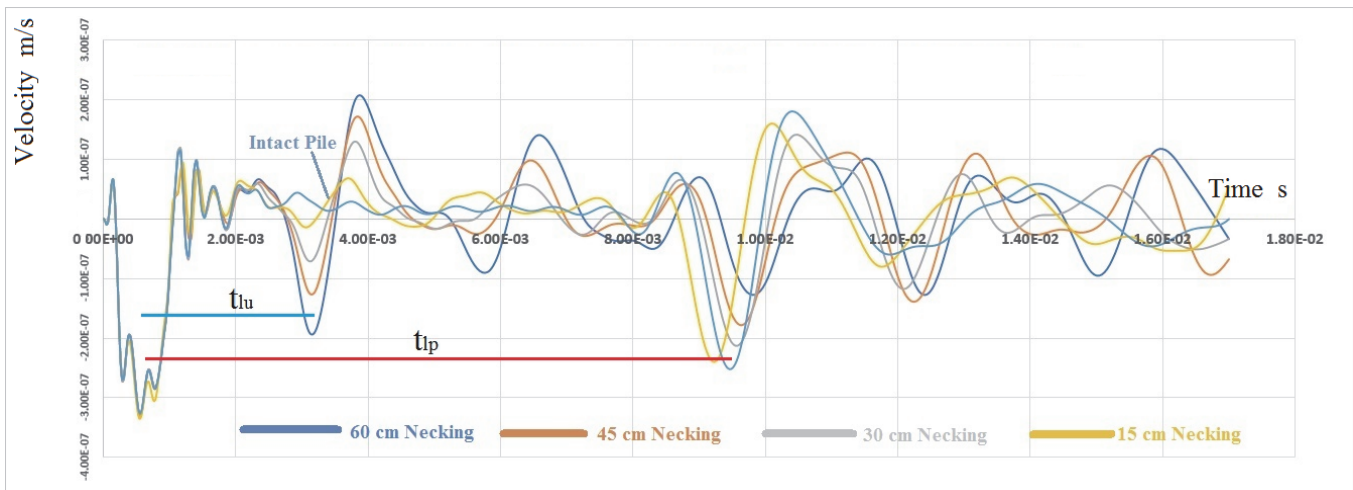
Figure 14: Velocity Response for an Intact Pile 120 cm Diameter Verses Four Defected Piles at the Upper Third of the Pile Length.

Fig. (15) presents a comparison of velocity time history between intact piles with D = 40, 60, 80, 100, and 120 cm. All five pile diameters have a common property, the response is always positive until it reaches the end of the pile, where reflection of the applied wave returns again. There is a relatively small shift between the end bottom parabola which may be due to noise that took place in the initial parabola.
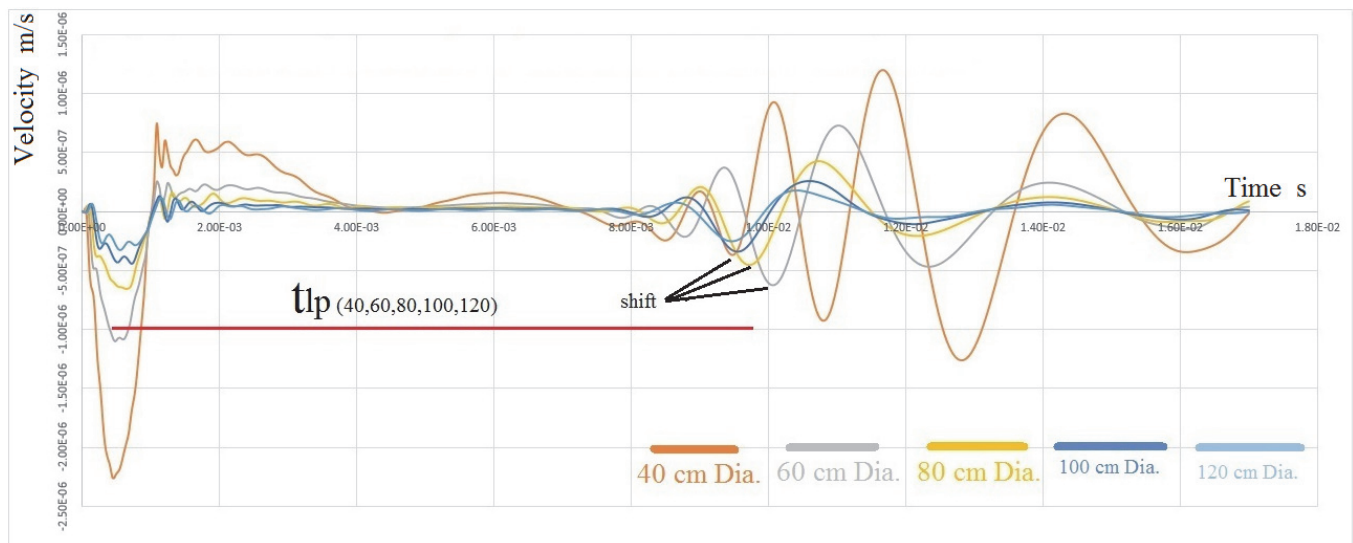

Figure 15: Velocity Response for Intact Piles of 40, 60, 80, 100, and 120 cm Diameter.

Fig. (16) presents a comparison of velocity time history between piles with D = 40, 60, 80, 100, and 120 cm through initial parabolas only. As shown, pile diameter of 40 cm has the deepest response and pile diameter of 120 cm has the shallowest. As the applied frequency is the same, the pile diameter effect is significant in the figure. The figure shows that frequency can be increased in piles of 100 and 120 cm diameter, which means results will be better, but its barely adjusted for piles of 40, 60 and may be present in pile diameter of 80 cm.
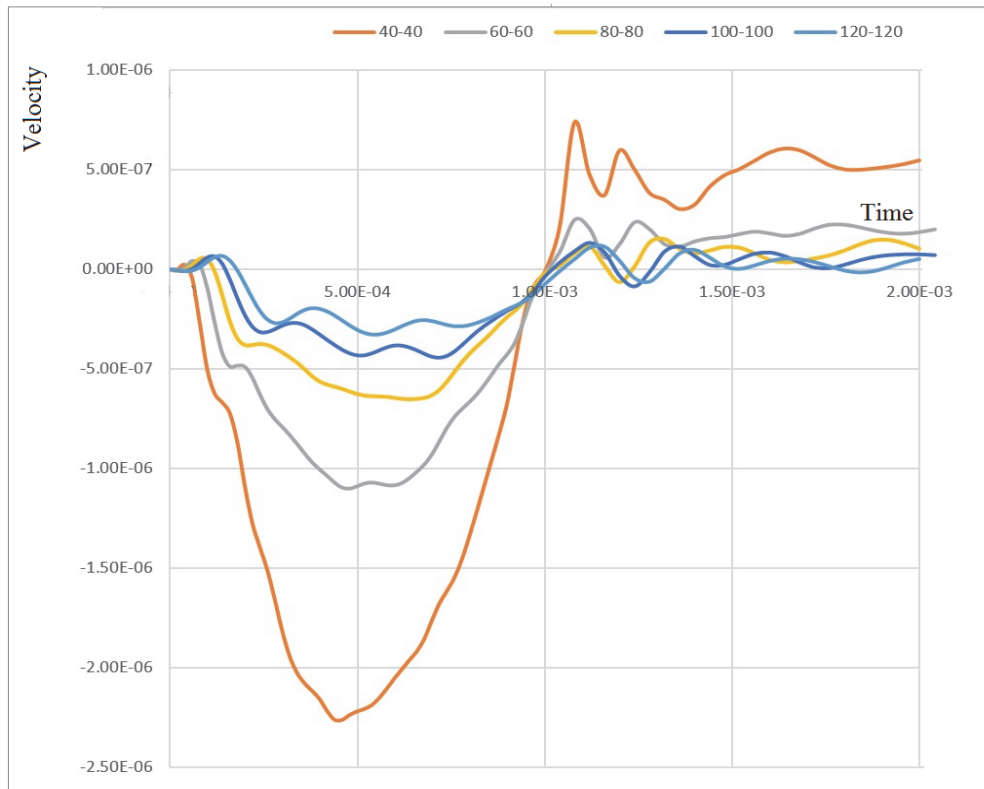
Figure 16: Velocity Response for Piles 40-60-80-100-120 cm Diameter Through Initial Parabola.

CONCLUSIONS

Concrete piles with and without defects under sinusoidal impact force with half kilo hertz frequency are studied using the finite element analysis software ADINA. The following conclusions are obtained from this study:

1-   There is an important zone of the velocity time history graph of the studied piles. This zone increases downward when the pile diameter decreases, or when the necking size increases for piles necked at their lower, middle, and upper parts.

2-   There is a similar time shift on the velocity time history diagram when the location of the necking moves from the pile top to the pile middle or the pile bottom.

3-   The distances between zones (Q), (P) and (O) are equal to the physical distances between the necking zones along the pile length.

4-   A new schematic diagram with details concerning the necking location and volume is identified. The introduced schematic diagram shows an initial parabola and a successive one. These two parabolas are the most significant ones along the solution time, as the damping tend to affect other parabolas along the pile length.

5-   For smaller pile diameters, the bottom of the parabola in the velocity time history graph is smoother with less noise meaning that the applied force fit well with smaller diameter piles than the larger ones.

6-   For intact piles, the distance between the peak of the initial parabolas and the successive one on the time domain is equivalent to the pile length when it is multiplied by half of the wave velocity.

7-   The ratio between the time difference along the peaks of the two initial parabolas, to the supposed travel time for an intact pile, is proportional to the ratio between the distance along the pile top to the necking zone, and the pile length. This relation could allocate the necking location along the pile length.

8-   The ratio between the time indicating the distance between the pile head and the upper necking zone and the time indicating the pile length is the same as the ratio between the time indicating distance between the first parabola and the total pile length in the intact pile.

9- The ratio between the necking diameter to the pile diameter values, is proportional to the ratio between the velocity value of the second parabola peak in the necked pile to the velocity value of the second one at the intact pile. The necking diameter also can be deduced from this mentioned ratio.

REFERENCE

[1] ADINA, (2021). Automatic Dynamic Incremental Nonlinear Analysis Software, Version 9.70, ADINA R & D, Watertown, MA, USA.

[2] Štrukelj, A., Pšunder, M., Vrecl-Kojc, H., and Trauner, L. (2009). Prediction of the Pile Behavior under Dynamic Loading Using Embedded Strain Sensor Technology, Acta Geotechnica Slovenica, 6, pp. 65-77.

[3] Ding, X., Liu, H., Liu, J., and Chen, Y., (2011). Wave Propagation in a Pipe Pile for Low-Strain Integrity Testing, Journal for Engineering Mechanics, 137, 9, pp.598-609.

[4] Li, Z. (2019). Torsional vibration of a large-diameter pipe pile embedded in inhomogeneous soil. Ocean Engineering, 172, pp. 737-758.

[5] Wu, J. T., Wang, K. H., Gao, L., and Xiao, S. (2019). Study on longitudinal vibration of a pile with variable sectional acoustic impedance by integral transformation. Acta Geotechnica, 14(6), pp. 1857-1870.

[6] Li, Z., and Gao, Y. (2019). Effects of inner soil on the vertical dynamic response of a pipe pile embedded in inhomogeneous soil. Journal of Sound and Vibration, 439, pp. 129-143.

[7] Hou, S.W., Hu, S.J., Guo, S.P., and Zeng, Y.Q., (2016). The Research of Multi-Defective Piles for Low Strain Testing and Numerical Simulation, In Structures Congress, 16°, Jeju Island, pp. 1-8.

[8] Cosic, M., Folic, B., and Folic, R. (2014). Numerical simulation of the pile integrity test on defected piles. Acta Geotechnica Slovenica, 11(2), pp. 5-19.

[9] Nazir, R., and El-Hussien, O., (2014). Mathematical Simulation of Pile Integrity Test (PIT), 4th International Conference on Geotechnique, Construction Materials and Environment, Brisbane, Australia, Nov. 19-21

[10] Niederleithinger, E., (2006). Numerical Simulation of Non-Destructive Foundation Pile Tests, The 9th European Conference on NDT, Berlin, Germany.

[11] Niederleithinger, E., (2008). Numerical Simulation of Low Strain Dynamic Pile Test, The 8th International Conference on the Application of Stress Wave Theory to Piles, Lisbon, Portugal, pp. 315-320.

[12] Joram M. Amir, (2009). Pile Integrity Testing, Pile test.com, 1st edition

[13] Warrington, D., Wynn, R., (2000). Comparison of Numerical Methods to Closed-Form Solution for Wave Equation Analysis of Piling, The 13th Annual Meeting of the Tennessee Section of the American Society of Civil Engineers, Smyrna, USA.

[14] Zhang, J., Liu, D.J., Geng, X., Gao, Z.J., Ke, Z.B., and Tao, J. (2016). Numerical Analysis of Low Strain Testing of 3-D Axial Symmetry Viscoelastic Pile–Soil Model, Indian Geotechnical Journal, 46(2), pp. 175-182.

[15] Zhang, C., Yang, S., Zhang, J., and Xiao, N., (2010). The Numerical Simulation for the Low Strain Dynamic Integrity Testing and Its Application in Quality Diagnosis of Foundation Pile, Journal of Xiamen University (Natural Science), Xiamen, China.